ACS APPLIED MATERIALS & INTERFACES

Research Article

Cite This: ACS Appl. Mater. Interfaces 2019, 11, 47422−47427

www.acsami.org

Microfiber Optic Arrays as Top Coatings for Front-Contact Solar Cells toward Mitigation of Shading Loss

Fu-Hao Chen, Saeid Biria, Hansheng Li, and Ian D. Hosein*

Department of Biomedical and Chemical Engineering, Syracuse University, Syracuse, New York 13244, United States

Supporting Information

ABSTRACT: Microfiber optic array structures are fabricated and employed as an optical structure overlaying a front-contact silicon solar cell. The arrays are synthesized through light-induced self-writing in a photo-crosslinking acrylate resin, which produces periodically spaced, high-aspect-ratio, and vertically aligned tapered microfibers deposited on a transparent substrate. The structure is then positioned over and sealed onto the solar cell surface. Their fiber optic properties enable collection of non-normal incident light, allowing the structure to mitigate shading loss through the redirection of incident light away from contacts and toward the solar cell. Angle-averaged external quantum efficiency increases nominally by 1.61%, resulting in increases in short-circuit current density up to 1.13 mA/cm^2. This work demonstrates a new approach to enhance light collection and conversion using a scalable, straightforward, light-based additive manufacturing process.

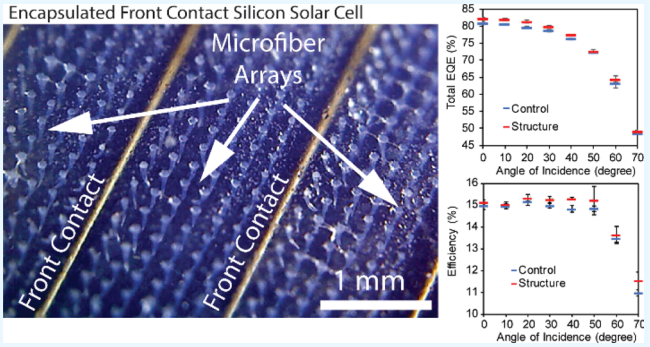

KEYWORDS: *solar cells, coatings, micropillar, fiber optic, self-writing, polymers, efficiency*

INTRODUCTION

In commercial standard solar cells, a specific optical loss is due to the shading effects owing to the metallic front contacts.[1,2] Shading accounts for more than 10% loss based on the fractional areal coverage by the front contacts over the solar cell surface, and losses increase with greater incident angle. Several approaches have been considered to mitigate contact losses, specifically through the implementation of optical effects via structuring of a top layer or coating the solar cell surface to manage light propagation and transmission. Such approaches have included nanoparticle surface coatings,[3] nanostructured diffractive, diffuse, and scattering layers,[4−7] gratings,[8] nanotexturing,[9] geometric optical structures,[5,10] more sophisticated methods such as contact cloaking,[11−13] and even, alternatively, back-contact architectures.[14] Particle coatings can be costly, wasteful, and complicated to predict and optimize. Diffractive and diffuse structures are wavelength- and angle-sensitive, and light scattering provides only partial relief from losses. Cloaking schemes drop in performance at greater incident angles, and the complexity and cost of back-contacts hinder their commercialization. Overall, the development of controllable, scalable material-based light-management solutions that are low-cost and wavelength-independent with wide angular windows of operation remains an open issue toward their viable integration into current solar cell manufacturing.

An attractive approach to mitigate shading losses is to employ broadband waveguide optics.[15] This has been most recently achieved using arrays of vertically aligned microscale broadband waveguides synthetically organized in polymer thin films that are overlaid onto the solar cell or directly processed over it.[15−17] The inherent angular acceptance range of the waveguides accepts non-normally incident light, which is thereafter transmitted along the waveguide directly to the solar cell to allow for increased conversion and current output at greater incident angles. Previous waveguide arrays have been explored in polymer blends that are organized into arrays of vertically aligned high-refractive-index cylindrical cores surrounded by a common low-refractive-index matrix.

In this work, we explore the synthesis and application of a microfiber array for increasing light collection and conversion in silicon solar cells. The fibers are fabricated through light-induced self-writing[18] in a photo-crosslinking acrylate system using arrays of microscale optical beams.[19−21] One advantage of employing a microfiber array is the significantly large refractive index difference between the fibers and the surrounding air, which leads to very large angular acceptance ranges, to thereby widen the angular collection range and to further mitigate shading loss. Owing to their large size (>10 μm), the microfibers are broadband, supporting the solar spectrum range to which silicon solar cells are responsive, namely the visible to near-infrared. Thus far, microfiber arrays (also referred to as micropillar arrays) have been predominantly employed for their inherent surface texture properties

Received: September 30, 2019
Accepted: November 22, 2019
Published: November 22, 2019

DOI: 10.1021/acsami.9b17803
ACS Appl. Mater. Interfaces 2019, 11, 47422−47427

in applications such as cell culture, antifouling, antiwetting, anti-icing, water collection, and better adhesion.[22−26] Jun et al. employed microfiber arrays specifically for vision optics, in which they leveraged the optical properties of the fibers.[27] Herein, this is the first time microfibers are used for light collection in solar cells. This approach is different from employing nanopillar arrays whose specific TE/TM optical modes are excited to elicit energy transfer.[28] Herein, optical energy is collected and transmitted in multimodal and multiwavelength form owing to the broadband nature of the micron-sized microfibers.

EXPERIMENTAL METHODS

Materials. Trimethylolpropane triacrylate (TMPTA) was purchased from Sigma-Aldrich. The visible-light photoinitiator system consisted of free-radical initiator camphorquinone (CQ) purchased from Sigma-Aldrich and cationic initiator (4-octyloxyphenyl)-phenyliodonium hexafluoroantimonate (OPPI) purchased from Hampford Research Inc. All chemicals were used as received.

Fabrication of Micropillar Array. Photocurable resins were prepared from a mixture of TMPTA with 1.5 wt % CQ and 2.5 wt %1 OPPI. Microfiber arrays were synthesized using irradiation from a collimated blue light-emitting diode (LED) (λ_{max} = 470 nm) combined with a mask pattern, as described previously.[19,20] The mask pattern combined (1) a chrome-based photomask consisting of a square array of apertures of 40 μm diameter and 200 μm spacing and (2) a printed mask (i.e., on a transparency film) consisting of parallel black lines of width 0.20 mm and 1.5 mm spacing. The irradiation intensity was 10 mW/cm^2, the exposure time was 20 min, and the resin thickness was 600 μm. After irradiation, the resin was thoroughly washed with ethanol and water and then dried in a vacuum oven at 45 °C overnight.

Assembly of the Photovoltaic Module. A planar multicrystalline silicon screen-printed solar cell (5 cm × 5 cm × 0.5 mm, front contact spacing = 1.5 mm) with a short-circuit current density of 35.5 mA/cm^2 was used. To assemble the waveguides on a solar cell, the substrate was turned over such that the microfibers were pointed toward and contacted with the solar cell, and the gaps in the arrays were aligned so as to be over the front contacts. The structure was hermetically sealed and fixed in place with adhesive tape. Optical microscopy images of the microfibers and the encapsulated solar cell were captured with a digital microscope (MicroView).

Solar Cell Measurements. External quantum efficiency (EQE) measurements were performed using a commercial measurement system (IQE 200B, Newport Inc.). The current density−voltage curves were measured using a solar simulator (94021A, Newport). Angle-resolved measurements were performed as described in our previous work.[17]

Ray-Tracing Simulations. Ray-tracing simulations were implemented by using the Advanced System Analysis Program (ASAP). Single-ray simulations were performed with different incident angles and different impinging locations in order to examine their interactions with a microfiber and a reflective metal contact. Details of the material parameters for the solar cell and contacts can be found elsewhere.[11]

RESULTS AND DISCUSSION

Operating Principles of the Microfiber Optic Array. Figure 1a shows a schematic of the microfiber array structure. The assembly approach is to position blocks of microfiber arrays over the silicon solar cell surface in between the front contacts. Given their greater height relative to the protruding contacts, via line of sight principles, non-normally incident light rays, otherwise ill-fated to impinge on the contacts, now interact with the top regions of the microfibers, enabling their collection and transmission within the fibers. Figure 1a schematically shows this favorable effect particularly for

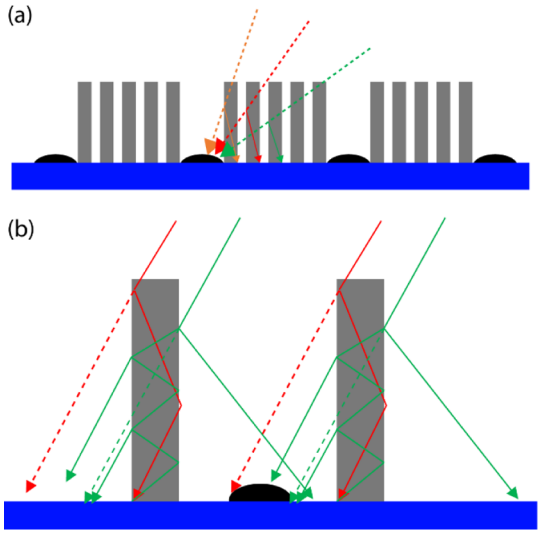

Figure 1. Proposed solar cell architecture consisting of microfiber arrays on the solar cell surface. (a) Schematic shows blocks of arrays positioned in the spaces between the metal contacts to collect and redirect non-normally incident light, otherwise ill-fated to hit the front contacts. (b) Exemplary ray tracing demonstrating the general operational principle of the waveguides, whereby a portion of light is collected by the waveguides and directed toward the solar cell. The red color rays show instances where light impinges on the top surface of the microfiber, and green rays show light impinging on the fibers' side walls. The results show how the fibers in the space between the metal contacts redirect light that would otherwise impinge on a contact. Solid rays show light when the structure is used. Dashed lines show unaltered pathways when no microfiber is in place.

microfibers in proximity to a front contact. Dashed lines indicate the unaltered light pathways if no microfiber is in place, and the solid lines show their altered pathways with the microfibers present. Figure 1b shows the detailed ray-tracing simulations, revealing how light may be collected at the top or side walls of the fibers and directed toward the solar cell (solid lines), as opposed to hitting the front contact (dashed lines). The range of incident angles that may be collected in this way is represented as the solid angular range $\Delta\theta$ of incoming light rays that satisfy the total internal reflection condition inside the fiber. The magnitude of $\Delta\theta$ is related to the refractive index values of the fiber (n_1) and the air surroundings (n_2 = 1) according to $\sin(\Delta\theta/2) = \sqrt{n_1^2 - n_2^2}$.[29] Using the refractive index value of photocured TMPTA (1.474, ref 9), a maximum acceptance range of 90° is possible, which is significantly larger than what is attainable from core−cladding architectures made from polymer blends (~30°).[16] Hence, all angles of incidence satisfy the total internal reflection condition inside the fiber. Hence, we are motivated to explore microfiber optic arrays owing to the significantly large refractive index difference between core and cladding, which can widen the angular acceptance range of the structure.

Structure Fabrication and Solar Cell Encapsulation. Figure 2a summarizes the steps to fabricate the microfiber arrays and their marriage to a front contact silicon solar cell. Using a casted resin over a plastic coverslip, the photomask is responsible for creating thousands of microscale optical beams, each of which will induce self-writing of a fiber in the resin. The additional printed mask attenuates strips of optical beams in the place intended to overlay the front contacts. The result is the self-writing of blocks of microfiber arrays, with ~200 μm

DOI: 10.1021/acsami.9b17803
ACS Appl. Mater. Interfaces 2019, 11, 47422−47427

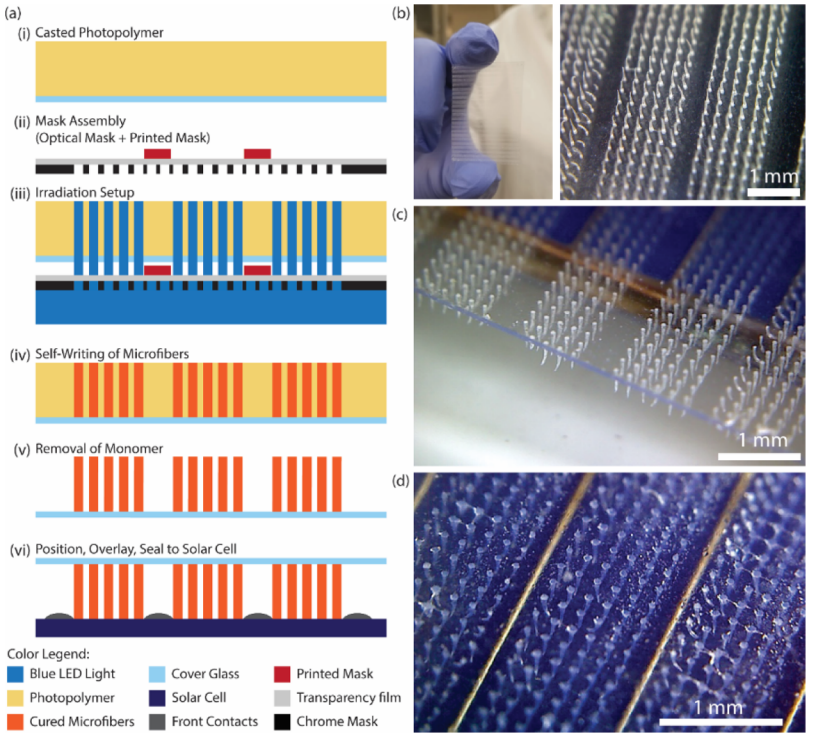

Figure 2. Fabrication of microfiber arrays for solar cell encapsulation. (a) Fabrication setup consists of a casted resin on a plastic substrate (i) and the mask pattern (photomask + printed mask) (ii) to produce blocks of microfiber arrays and to allow space for the protrusion of the screen-printed front contacts. The resin is irradiated from below with blue collimated LED light that induces self-writing of the microfiber arrays (iii,iv). The sample is washed to leave the blocks of microfiber arrays adhered to the plastic substrate (v) and is then turned over and aligned and fixed to the solar cell (vi). (b) Images of the blocks of microfiber arrays produced on the plastic substrate. (c) Microscope images of the microfiber array structure overlaying the solar cell, offset for the purpose of clarity on its position and alignment. (d) Microscope image of the final encapsulated structure over the solar cell. The positions of the blocks of microfiber arrays in between the front contacts can be clearly observed.

gaps in between blocks, which are extracted from the irradiated resin after removal of the uncured monomer through washing. The fibers are tapered, with a midlength diameter of approximately 40 μm and an average height of 466 μm. The diameter is large enough to support multiwavelength and multimodal light propagation, and the tapered waveguide profile is suitable for light guiding.[30] The microfibers are reasonably transparent, as determined in our previous work with TMPTA microfibers,[19] in order to demonstrate their effectiveness for light management. The microfiber array structure adhered to its plastic substrate is then overturned, laid over, and aligned over the silicon solar cell surface. Figure 2b shows the blocks of microfibers produced over the plastic substrate (sample size 2.5 × 3.5 cm), and high magnification optical microscopy reveals their highly ordered and vertically aligned arrangement in each block. Figure 2c shows the structure placed and aligned over the silicon solar cell surface, but slightly offset to visually delineate the appearance of the overturned fibers and their appearance when overlaid on the solar cell surface. Figure 2d shows the well-positioned microfiber arrays in between the contacts in the encapsulated cell. The plastic coverslip acts as the final cover layer which completes the encapsulation. While plastic is used herein, the microfibers may also be deposited on glass substrates as the final cover layer.[19]

EQE Measurements. EQE spectra from 350 to 1100 nm are shown in Figure 3a,b. The control with which we make comparisons to the microfiber array (herein referred to as the "structure") is the same plastic substrate without microfibers overlaid on the solar cell. The maximum EQE of the structures reaches 89.76% at normal incidence (89.00% for the control), demonstrating an improvement even for normal incidence light. While designed herein to provide enhanced performance at non-normally incident angles, the small increase at normal incidence may be attributed to the concentrating properties of the waveguides as well as possible additional scattering of light at the air−fiber interfaces, particularly when incident light scatters off the solar cell, which can provide more opportunities for light to return to the solar cell for further collection. With increased angle of incidence, the drop in the EQE spectra, a trend indicative of shading loss, is abated when the structure is employed. In order to clearly observe this improvement, the spectrally averaged EQE was calculated according to

$$\text{average EQE} = \frac{\int \phi(\lambda)\cdot \text{EQE}(\lambda)\,d\lambda}{\int \phi(\lambda)\,d\lambda} \times 100\% \quad (1)$$

where $\phi(\lambda)$ is the photon flux of AM 1.5 G at a wavelength, λ. Plots of this average (total) EQE over incident angle are shown in Figure 2c. Overall, the structure yields a higher average EQE than the control, which indicates that it enhances the collection and conversion efficiency over the angular range of incidence from 0 to 70°. The difference in the total EQE between the structure and the control (Figure 3c, inset) shows its nominal value being stable up to 40°, whereafter variations begin, owing to the extreme glancing angle of incidence and complex interactions (i.e., collection and reflection) with the structure under these conditions.

To reveal the overall performance across all angles, the angularly averaged EQE was calculated according to

DOI: 10.1021/acsami.9b17803
ACS Appl. Mater. Interfaces 2019, 11, 47422−47427

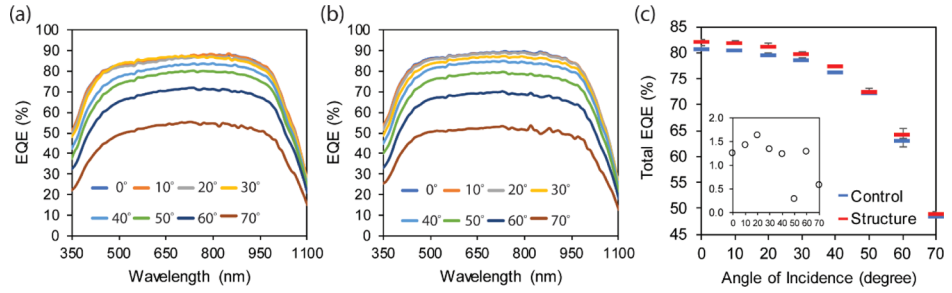

Figure 3. EQE spectra of (a) the control and (b) the structure. EQE of the structure is higher than that of the control. (c) Spectral average (total) EQE plotted as a function of the incident angle, which shows consistently higher values for the structure over the control. EQE error bars shown are standard deviations of three different samples measured. The inset shows nominal change in the total EQE for the structure with respect to the control.

$$\mathrm{EQE}_{\mathrm{ave}} = \frac{\sum_{\theta} \mathrm{EQE}(\theta)\cos(\theta)}{\sum_{\theta} \cos(\theta)} \tag{2}$$

where θ is the incident angle and the $\cos(\theta)$ term accounts for the reduced photon flux with increasing incident angle. This calculated average EQE for the structure and control was 76.7 and 75.48%, respectively, yielding 1.61% improvement which indicates that an overall angular-based performance enhancement is achieved with the use of the microfiber array structure.

In terms of wavelength-specific enhancements, the largest nominal increases in EQE are observed for shorter wavelengths (see the Supporting Information). Up to an angle of incidence of 40°, increases in EQE across the entire wavelength range are observed. For angles of incidence of 50−70°, nominal percent enhancements are only observed in the short wavelength range (less than ∼550 nm). Improved EQE at shorter wavelengths, especially at higher incident angles, may be owing to the increased number of optical modes supported by the fiber and the greater acceptance range ($\Delta\theta$), both of which increase with smaller wavelength,[29] thereby allowing shorter wavelength light to be more easily collected and transmitted through the fibers.

***J*−*V* Measurement and Solar Cell Efficiency.** The current density against voltage (J−V) curves as well as plots of the short-circuit current density (J_{SC}) and solar cell efficiency are shown in Figure 4. J_{SC} also shows a characteristic drop with increased incident angle associated with shading. However, J_{SC} shows enhancements over the entire range of incident angles investigated when the structure is employed (Figure 4c). Nominal increases to J_{SC} were in the range of 0.36−1.13 mA/cm^2; or in terms of percentages, increases over the control were 1.6−4.8% (greatest % increase at 70°). The solar cell efficiency plot shows a trend of increase in nominal enhancement in efficiency up to 40°, with a drop for 50 and 60° (yet still positive) and then a strong enhancement at the largest incident angle, 70°. Importantly, increases in efficiency are observed over the entire angular range, with nominal enhancements in the range of 0.10−0.56% (greatest at 70°). The variation in the magnitude of the enhancement shows a similar trend over incident angle as J_{SC} (insets of Figure 4c,d). The results indicate that the structure enables the collection and conversion of more light and sustains a greater solar cell efficiency and current output over the entire angular range. In order to clearly reveal the enhancement in solar cell efficiency, the angularly averaged solar cell efficiency was determined according to

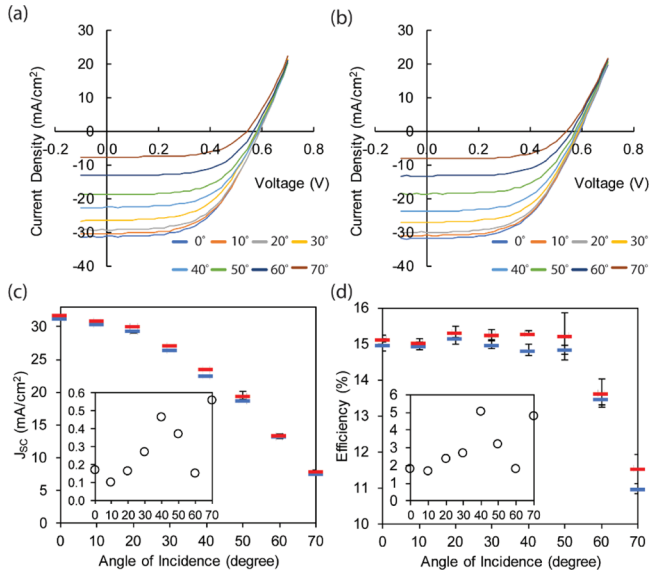

Figure 4. J−V curves of the (a) control and (b) structure. (c) Plots of J_{SC} as a function of the angle, extracted from the J−V curves, which shows an enhancement over the entire angular incidence range. (d) Solar cell efficiency as a function of the angle of incidence, which also shows enhancement over the entire range. Y-axis error bars shown in (c,d) are standard deviations of three different samples measured. Insets of (c,d) show percent increases for the structure with respect to the control.

$$\eta_{\mathrm{ave}} = \frac{\sum_{\theta} \eta(\theta)\cos(\theta)}{\sum_{\theta} \cos(\theta)} \tag{3}$$

where $\eta(\theta)$ is the solar cell efficiency herein as a function of the incident angle, θ. The calculated efficiency values were 14.86 and 14.61% for the structure and the control, respectively, and hence the structure improves efficiency by 1.71%.

Trends in the increase of the solar cell efficiency and current output can be understood in terms of the interactions of light with the microfibers. From 0 to 40°, as the shading effect of the solar cell increases, the capability of the microfibers to mitigate this loss through collecting and redirecting light becomes more pronounced. However, at even greater angles (50−60°), it is possible that the strong refractive index difference between the pillars and air (Δn = 0.474) leads to strong reflection/scattering of light off the microfiber walls, which might not be as efficient for collection, hence a slight drop in performance (yet an improvement is still attained). At a very large incident angle of 70°, this scattering is favorable over the otherwise

DOI: 10.1021/acsami.9b17803
ACS Appl. Mater. Interfaces 2019, 11, 47422−47427

significant shading loss, resulting in a large nominal increase in the efficiency. Importantly, all performance enhancements are greater than achieved for a uniform resin encapsulant,[15] as well as for a waveguide array produced from polymer blends,[17] namely a microfiber embedded in the matrix of another polymer, indicating that the strong refractive index difference achieved with the fiber−air interface is favorable. Trends in the differences in the total EQE, J_{SC}, and power conversion efficiency do not necessarily correlate owing to the different conditions of the EQE and J_{SC}/η measurements. What can be stated is that the total EQE is sustained up to 40°, and the J_{SC}/η increases owing to the pronounced favorable effect of the pillars with increased angle of incidence.

Based on the lineal fraction of the microfibers and line of sight principles, the microfibers would only capture one-fifth of the light owing to the ∼40 μm diameter, spaced 200 μm apart, which is a sparse density of fibers in the array. The lineal fraction dependence is confirmed by the fact that the shading loss is around 10%, so the structures could recover maximally 2% of this lost light. Comparing with the experimental gain of 1.71%, the results are quite close to the upper limit, indicating that this microfiber array structure is an efficient approach to recover shading losses, even at very large incident angles, and that there are opportunities for further enhancement via array design. Denser micropillar arrays as well as nonsquare arrangements will be explored in structural optimization studies to determine the best fiber spacing to maximize performance enhancement, which will be reported in the future.

CONCLUSIONS

To achieve wide-angle light capture to recover light lost from shading, a top-coating consisting of blocks of microfiber arrays were fabricated, and encapsulated solar cells were tested for performance enhancement. Owing to the collecting and light-guiding capabilities of the microfibers, the arrays enable the capture and redirection of light toward the solar cell that would otherwise be lost owing to it hitting the front contacts. Enhancements in the EQE, short-circuit current density, and solar cell efficiency are observed. The practical implication of this work is that with this structural approach, solar cell efficiency and current output can be enhanced over a large angular range. This has the potential to translate to greater energy conversion as the sun travels its varying diurnal trajectories during the day as well as over the course of seasons.

ASSOCIATED CONTENT

Supporting Information

The Supporting Information is available free of charge at https://pubs.acs.org/doi/10.1021/acsami.9b17803.

Plots of EQE difference between structure and control as a function of the wavelength over all angles of incidence (PDF)

AUTHOR INFORMATION

Corresponding Author

*E-mail: idhosein@syr.edu.

ORCID

Ian D. Hosein: 0000-0003-0317-2644

Notes

The authors declare no competing financial interest.

ACKNOWLEDGMENTS

The authors gratefully acknowledge funding from the National Science Foundation (CMMI-1751621 and DMR-1903592) as well as support from the College of Engineering and Computer Science at Syracuse University.

REFERENCES

(1) Weber, K. J.; Everett, V.; Deenapanray, P. N. K.; Franklin, E.; Blakers, A. W. Modeling of Static Concentrator Modules Incorporating Lambertian or V-Groove Rear Reflectors. *Sol. Energy Mater. Sol. Cells* **2006**, *90*, 1741−1749.

(2) Stuckings, M. F.; Blakers, A. W. A Study of Shading and Resistive Loss from the Fingers of Encapsulated Solar Cells. *Sol. Energy Mater. Sol. Cells* **1999**, *59*, 233−242.

(3) Cheng, T.-D.; Chen, Y.-P.; Chen, P.-C. Efficiency Improvement of Photovoltaic Module Via Grid Diffusers in Eva Encapsulation Layer. *Proceedings of the 27th European Photovoltaic Solar Energy Conference and Exhibition*, 2012; pp 333−334.

(4) Xu, Q.; Meng, L.; Wang, X. Reducing Shadowing Losses in Silicon Solar Cells Using Cellulose Nanocrystal: Polymer Hybrid Diffusers. *Appl. Opt.* **2019**, *58*, 2505−2511.

(5) Jaus, J.; Pantsar, H.; Eckert, J.; Duell, M.; Herfurth, H.; Doble, D. Light Management for Reduction of Bus Bar and Gridline Shadowing in Photovoltaic Modules. *35th IEEE Photovoltaic Specialists Conference*, 2010; Vol. *35*, pp 979−983.

(6) Ebner, R.; Schwark, M.; Kubicek, B.; Újvári, G.; Mühleisen, W.; Hirschl, C.; Neumaier, L.; Pedevilla, M.; Scheurer, J.; Plösch, A.; Kogler, A.; Krumlacher, W.; Muckenhuber, H. Increased Power Output of Crystalline Silicon Pv Modules by Alternative Interconnection Applications, *Proceedings of the 28th European Photovoltaic Solar Energy Conference and Exhibition*, 2013; pp 489−494.

(7) Mingareev, I.; Berlich, R.; Eichelkraut, T. J.; Herfurth, H.; Heinemann, S.; Richardson, M. C. Diffractive Optical Elements Utilized for Efficiency Enhancement of Photovoltaic Modules. *Opt. Express* **2011**, *19*, 11397−11404.

(8) Kim, Y. J.; Yoo, Y. J.; Yoo, D. E.; Lee, D. W.; Kim, M. S.; Jang, H. J.; Kim, Y.-C.; Jang, J.-H.; Kang, I. S.; Song, Y. M. Enhanced Light Harvesting in Photovoltaic Devices Using an Edge-Located One-Dimensional Grating Polydimethylsiloxane Membrane. *ACS Appl. Mater. Interfaces* **2019**, *11*, 36020−36026.

(9) van Deelen, J.; Tezsevin, Y.; Omar, A.; Xu, M.; Barink, M. Benefit of Textured Cigs Cells for Low Reflecting Nanogrid Application. *MRS Advances* **2017**, *2*, 3175−3180.

(10) Lin, H.; Biria, S.; Chen, F.-H.; Hosein, I. D.; Saravanamuttu, K. Waveguide-Imprinted Slim Polymer Films: Beam Steering Coatings for Solar Cells. *ACS Photonics* **2019**, *6*, 878−885.

(11) Chen, F.-h.; Pathreeker, S.; Kaur, J.; Hosein, I. D. Increasing Light Capture in Silicon Solar Cells with Encapsulants Incorporating Air Prisms to Reduce Metallic Contact Losses. *Opt. Express* **2016**, *24*, A1419−A1430.

(12) Schumann, M. F.; Langenhorst, M.; Smeets, M.; Ding, K.; Paetzold, U. W.; Wegener, M. All-Angle Invisibility Cloaking of Contact Fingers on Solar Cells by Refractive Free-Form Surfaces. *Adv. Opt. Mater.* **2017**, *5*, 1700164.

(13) Langenhorst, M.; Ritzer, D.; Kotz, F.; Risch, P.; Dottermusch, S.; Roslizar, A.; Schmager, R.; Richards, B. S.; Rapp, B. E.; Paetzold, U. W. Liquid Glass for Photovoltaics: Multifunctional Front Cover Glass for Solar Modules. *ACS Appl. Mater. Interfaces* **2019**, *11*, 35015−35022.

(14) Kerschaver, E. V.; Beaucarne, G. Back-Contact Solar Cells: A Review. *Prog. Photovoltaics* **2006**, *14*, 107−123.

(15) Biria, S.; Chen, F. H.; Pathreeker, S.; Hosein, I. D. Polymer Encapsulants Incorporating Light-Guiding Architectures to Increase Optical Energy Conversion in Solar Cells. *Adv. Mater.* **2017**, *30*, 1705382.

(16) Biria, S.; Chen, F.-H.; Hosein, I. D. Enhanced Wide-Angle Energy Conversion Using Structure-Tunable Waveguide Arrays as

DOI: 10.1021/acsami.9b17803
ACS Appl. Mater. Interfaces 2019, 11, 47422−47427

Encapsulation Materials for Silicon Solar Cells. *Phys. Status Solidi A* **2019**, *216*, 1800716.
(17) Biria, S.; Wilhelm, T. S.; Mohseni, P. K.; Hosein, I. D. Direct Light-Writing of Nanoparticle-Based Metallo-Dielectric Optical Waveguide Arrays over Silicon Solar Cells for Wide-Angle Light Collecting Modules. *Adv. Opt. Mater.* **2019**, *7*, 1900661.
(18) Biria, S.; Morim, D. R.; An Tsao, F.; Saravanamuttu, K.; Hosein, I. D. Coupling Nonlinear Optical Waves to Photoreactive and Phase-Separating Soft Matter: Current Status and Perspectives. *Chaos* **2017**, *27*, 104611.
(19) Li, H.; Chen, F.-H.; Biria, S.; Hosein, I. D. Prototyping of Superhydrophobic Surfaces from Structure-Tunable Micropillar Arrays Using Visible Light Photocuring. *Adv. Eng. Mater.* **2019**, *21*, 1801150.
(20) Chen, F. H.; Pathreeker, S.; Biria, S.; Hosein, I. D. Synthesis of Micropillar Arrays Via Photopolymerization: An in Situ Study of Light-Induced Formation, Growth Kinetics, and the Influence of Oxygen Inhibition. *Macromolecules* **2017**, *50*, 5767−5778.
(21) Biria, S.; Malley, P. P. A.; Kahan, T. F.; Hosein, I. D. Tunable Nonlinear Optical Pattern Formation and Microstructure in Cross-Linking Acrylate Systems During Free-Radical Polymerization. *J. Phys. Chem. C* **2016**, *120*, 4517−4528.
(22) Golovin, K.; Lee, D. H.; Mabry, J. M.; Tuteja, A. Transparent, Flexible, Superomniphobic Surfaces with Ultra-Low Contact Angle Hysteresis. *Angew. Chem., Int. Ed.* **2013**, *52*, 13007−13011.
(23) Lee, S. Y.; Rahmawan, Y.; Yang, S. Transparent and Superamphiphobic Surfaces from Mushroom-Like Micropillar Arrays. *ACS Appl. Mater. Interfaces* **2015**, *7*, 24197−24203.
(24) Zhang, H.; Bian, C.; Jackson, J. K.; Khademolhosseini, F.; Burt, H. M.; Chiao, M. Fabrication of Robust Hydrogel Coatings on Polydimethylsiloxane Substrates Using Micropillar Anchor Structures with Chemical Surface Modification. *ACS Appl. Mater. Interfaces* **2014**, *6*, 9126−9133.
(25) Fan, Z.; Zhang, W.; Fu, Y.; Yan, L.; Ma, X. Facile Synthesis of Silicon Micropillar Arrays Using Extreme Ultraviolet Lithography and Ag-Assisted Chemical Etching Method. *J. Phys. Chem. C* **2016**, *120*, 6824−6834.
(26) Miller, K.; Li, M.; Walsh, K. M.; Fu, X.-A. The Effects of Drie Operational Parameters on Vertically Aligned Micropillar Arrays. *J. Micromech. Microeng.* **2013**, *23*, 035039.
(27) Jun, B. M.; Serra, F.; Xia, Y.; Kang, H. S.; Yang, S. Fabrication of Free-Standing, Self-Aligned, High-Aspect-Ratio Synthetic Ommatidia. *ACS Appl. Mater. Interfaces* **2016**, *8*, 30671−30676.
(28) Fan, Z.; Ruebusch, D. J.; Rathore, A. A.; Kapadia, R.; Ergen, O.; Leu, P. W.; Javey, A. Challenges and Prospects of Nanopillar-Based Solar Cells. *Nano Res.* **2009**, *2*, 829−843.
(29) Saleh, B. E. A.; Teich, M. C. Guided-Wave Optics. *Fundamentals of Photonics*; John Wiley & Sons, Inc., 2001.
(30) Frisken, S. J. Light-Induced Optical Waveguide Uptapers. *Opt. Lett.* **1993**, *18*, 1035−1037.

DOI: 10.1021/acsami.9b17803
ACS Appl. Mater. Interfaces 2019, 11, 47422−47427